Carbon Dots Embedded in Cellulose Film

Programmable, Performance-Tunable, and Large-Scale Subtle Fluorescent Patterning by in Situ Laser Writing

Guo, Yuanyuan; Wang, Quan; Li, Hao; Gao, Yixun; Xu, Xuezhu; Tang, Biao; Yang, B.; Lee, Yi Kuen; French, Paddy J.; More Authors

DOI
10.1021/acsnano.1c09999

Publication date
2022

Document Version
Final published version

Published in
ACS Nano

Citation (APA)
Guo, Y., Wang, Q., Li, H., Gao, Y., Xu, X., Tang, B., Yang, B., Lee, Y. K., French, P. J., & More Authors (2022). Carbon Dots Embedded in Cellulose Film: Programmable, Performance-Tunable, and Large-Scale Subtle Fluorescent Patterning by in Situ Laser Writing. *ACS Nano*, *16*(2), 2910-2920. https://doi.org/10.1021/acsnano.1c09999

ACS NANO

www.acsnano.org

ARTICLE

Carbon Dots Embedded in Cellulose Film: Programmable, Performance-Tunable, and Large-Scale Subtle Fluorescent Patterning by *in Situ* Laser Writing

Yuanyuan Guo, Quan Wang, Hao Li, Yixun Gao, Xuezhu Xu, Biao Tang, Yao Wang,* Bai Yang, Yi-Kuen Lee, Paddy J. French, and Guofu Zhou

Cite This: *ACS Nano* 2022, 16, 2910−2920

Read Online

ACCESS | Metrics & More | Article Recommendations | Supporting Information

ABSTRACT: **Fluorescent patterns with multiple functions enable high-security anti-counterfeiting labels. Complex material synthesis and patterning processes limit the application of multifunctional fluorescent patterns, so the technology of *in situ* fluorescent patterning with tunable multimodal capabilities is becoming more necessary. In this work, an *in situ* fluorescent patterning technology was developed using laser direct writing on solid cellulose film at ambient conditions without masks. The fluorescent intensity and surface microstructure of the patterns could be adjusted by programmable varying of the laser parameters simultaneously. During laser direct writing, carbon dots are generated *in situ* in a cellulose ester polymer matrix, which significantly simplifies the fluorescent patterning process and reduces the manufacturing cost. Interestingly, the tunable fluorescent intensity empowers the fabrication of visual stereoscopic fluorescent patterns with excitation dependence, further improving its anti-counterfeiting performance. The obtained fluorescent patterns still show ultrahigh optical properties after being immersed in an acid/base solution (pH 5−12) over one month. In addition, the anti-UV performance of the obtained laser-patterned film with transmittance around 90% is comparable to that of commercial UV-resistant films. This work provided an advanced and feasible approach to fabricating programmable, performance-tunable, subtle fluorescent patterns in large-scale for industrial application.**

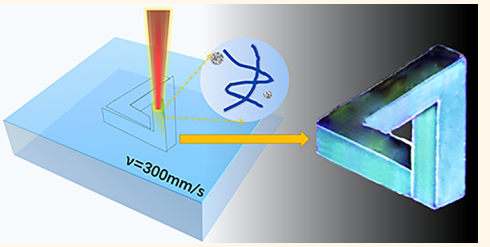

KEYWORDS: *fluorescent pattern, tunable intensity, surface microstructure, laser direct writing, carbon dots*

Subtle patterning with specific optical and structural characteristics has promising applications, including bioengineering, anti-counterfeiting, information storage, and sensors.[1−8] Fluorescent patterns have advantages for applications in sensing and anti-counterfeiting. In general, fluorescent patterns were made using fluorescent materials with poor biocompatibility, such as fluorescent dyes, quantum dots, and rare earth nanomaterials.[9−13] A predesigned mask or an appropriated ink formulation has to match the patterning processes (UV radiation or inkjet print), which increases the cost and complexity of the entire process.[14−17] Therefore, a high-efficiency *in situ* fluorescent patterning process based on nontoxic materials with tunable multimode functions becomes more important and attractive for researchers in the field of anti-counterfeiting. It is known that the combination of tunable fluorescence and surface structure is one of the efficient ways to enhance the anti-counterfeiting performance of the fluorescent patterns.[18,19] Ma et al. invented an intelligent surface with dynamic hierarchical wrinkles and fluorescence using a supramolecular network comprising a copolymer captaining pyridine (P4VP-*n*BA-S) and hydroxyl distyrylpyridine (DSP-OH).[1] Although the dynamic dual-function pattern exhibits random wrinkled topography and fluorescence simultaneously, it is challenging to exactly reproduce the surface microstructure on different samples in their work, which inhibits the large-scale production of anti-counterfeiting labels. Hence, a technique for subtle patterning with controllable and reproducible microstructure is demanded by practical applications.

It is known that laser direct writing technology is the most high-efficiency way to fabricate 3D micro-/nanostructure

Received: November 11, 2021
Accepted: January 31, 2022
Published: February 3, 2022

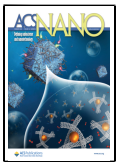

arrays on a large scale.[20,21] Especially, it has widely been used for patterning or architecting polymer materials.[22−27] In recent years, polymer-based laser direct writing technology has attracted tremendous interest and has commonly been utilized to fabricate microfluidic channels, optical waveguides, flexible electronics, *etc.*[28−31] Meanwhile, ablation during laser radiation also provides more possibility to *in situ* synthesize functional fluorescent materials.[32−35] Typically, Smalyukh et al. used femtosecond lasers to reduce graphene sheets in discotic liquid crystal gels, successfully creating 3D fluorescent solid microstructures and patterns.[12] Similarly, Dong et al. produced 2D and 3D fluorescent patterns using *in situ* forming perovskite quantum dots inside glass by a femtosecond laser, which is promising in high-capacity optical data storage and information encryption.[36] In particular, fluorescence patterns could be formed by laser direct writing on rare metallic nanoparticle composited polymers such as Ag/PVA and Au/PVA composites, but it is impossible to build subtle microstructures on the surface of the patterns.[37−40] Unlike sensitive perovskite-based and precious metal composited materials, fluorescent patterning on common polymers will have promising prospects. To the best of our knowledge, fluorescent patterning by laser direct writing on a cheap, accessible, and single-component polymer is rarely reported.[41,42]

Nowadays, finding carbon dots (CDs) has added a fresh stream to the fluorescence materials family.[43−45] It is time-consuming to synthesize CDs, and the yield was normally low, which made CDs very expensive. The patterning of CDs was usually involved in redistributing pure CDs in a particular medium followed with a multistep process, which limited its large-scale application.[46] Through the laser direct writing process, a pattern can be synthesized *in situ* in one step in the demanded area, which would robustly increase the patterning efficiency. As a biocompatible polymer, cellulose is a well-known source to prepare CDs and fluorescence polymers,[47−52] but no one has tried to obtain CDs by laser ablating cellulosic polymers. Considering its outstanding optical, film-forming, thermal, and chemical properties, cellulose acetate butyrate (CAB) was selected for *in situ* fluorescent patterning in this work. A series of subtle fluorescent patterns with a tunable "fingerprint" microstructure were prepared by laser direct writing on a CAB film. The intensity of the fluorescent pattern and the microstructure on the patterned surface can be regulated simultaneously by modulating the laser direct writing parameters. We confirmed that the fluorescence of the patterns originated from CDs generated *in situ* in CAB films. The transformation of CAB into CDs was attributed to the laser irradiation-induced photothermal effect. In addition, while retaining the polymer properties of CAB, laser direct writing enables dual-function fluorescent patterns on the CAB film. The obtained fluorescence patterns had higher anti-counterfeiting performance and showed promising prospects for application.

RESULTS AND DISCUSSION

***In Situ* Fluorescence Patterning by Laser Direct Writing.** A mid-IR laser (CO_2 laser) can effectively carbonize polymer materials to produce functional materials.[53,54] In this work, a CO_2 pulsed laser (wavelength 10.6 μm) with a line scanning function was chosen to draw fluorescent patterns on the surface of the CAB film. The peak power during laser direct writing can reach 8 kW with a pulse energy of 0.16 mJ (energy density of 8.15 J/cm^2). The single pulsed laser etched depth was decreased with decreasing fluence, and the threshold energy density was 1.63 J/cm^2 (20% power) for CAB (10 μm film) (Figure S1i). Considering the thickness of the CAB film (5 ± 1 μm) from 10 wt % solutions and a broader scan rate range, the power for drawing fluorescent patterns was estimated to be 4 W, which was below the threshold energy density. The laser machine we used has the most stable output at a frequency of 25 kHz; thus, all experiments in this work were carried out under laser power 4 W and frequency 25 kHz.

As illustrated in Figure 1b (inset image), these lines are formed by setting the distance between two adjacent spots center equal to the radius of the spot. The areas of the CAB surface exposed to the programming-controlled laser beam were converted into fluorescent patterns, while the unexposed area remained unchanged (Figure 1b,c). With the help of computer controlling, fluorescent patterns of various geometric shapes can be drawn quickly on CAB film according to predesign graphs (Figure 1h).

We systematically investigated the relationship between optical property and the laser writing parameter to optimize the photoluminescent properties of fluorescent patterns. Our experiments found that the fluorescent intensity was related to the scan rate and line spacing. With fixed line spacing (0.02 mm), the fluorescent intensity could be regulated by varying the scan rate from 800 to 1400 mm/s (Figure 1a). The fluorescent intensity increased with scan rate (700−1000 mm/s), and it decreased as soon as the scan rate was higher than 1000 mm/s (Figure 1e). The maximum emission wavelength was 450 nm excited by 360 nm and did not shift with the scan rate. No fluorescence was observed when the scan rate exceeded 1500 mm/s due to low adsorbed energy. The highest fluorescent intensity was formed at a scan rate of 1000 mm/s with 0.02 mm line spacing. Under this condition, an SCNU school badge (2 × 2 cm^2) could be drawn within 20 s (Figure 2i inset). There was pyrolysis gas emission during the laser writing process; more extensive gas emission was observed because more energy was absorbed by the unit area at a lower scan rate (Figure S1). The scan rate range for generating the fluorescent pattern was also different for different line spacing settings. The maximum intensity peak appeared at different scan rates (Figure 1g). For instance, the fluorescent intensity could be varied by changing the laser scan rate in the range from 80−300 mm/s for 0.1 mm line spacing, where the scan rate range was 300−500 mm/s for 0.05 mm line spacing, respectively.

According to the literature, the etch depth was related to laser ablation time. The etching process occurred layer by layer on the polymer surface.[24] The "fingerprint" surface microstructures were achieved by varying the scan rate with the line spacing wider than the diameter of a single laser pulse spot (50 ± 5 μm). The height of the line structure increased from 0.5 μm (80 mm/s) to 3 μm (200 mm/s) with increasing fluorescent intensity at 0.1 mm line spacing (Figure 1d-i,ii). The longer drawing time induced by a slow scan rate resulted in more laser pulse per unit area; thus, more material on the CAB surface was ablated. During laser writing on the surface of CAB film, emission gas and some short-chain molecules would burst from the surface and absorb part of the laser energy. Together with the quick heat transfer between the air, film, and the glass substrate, the molten material solidified as soon as the laser beam left, resulting in a fluorescent pattern with line structures. Most of the CAB was vaporized by laser-induced photolysis at a lower scan rate (80 mm/s), resulting in

https://doi.org/10.1021/acsnano.1c09999
ACS Nano 2022, 16, 2910−2920

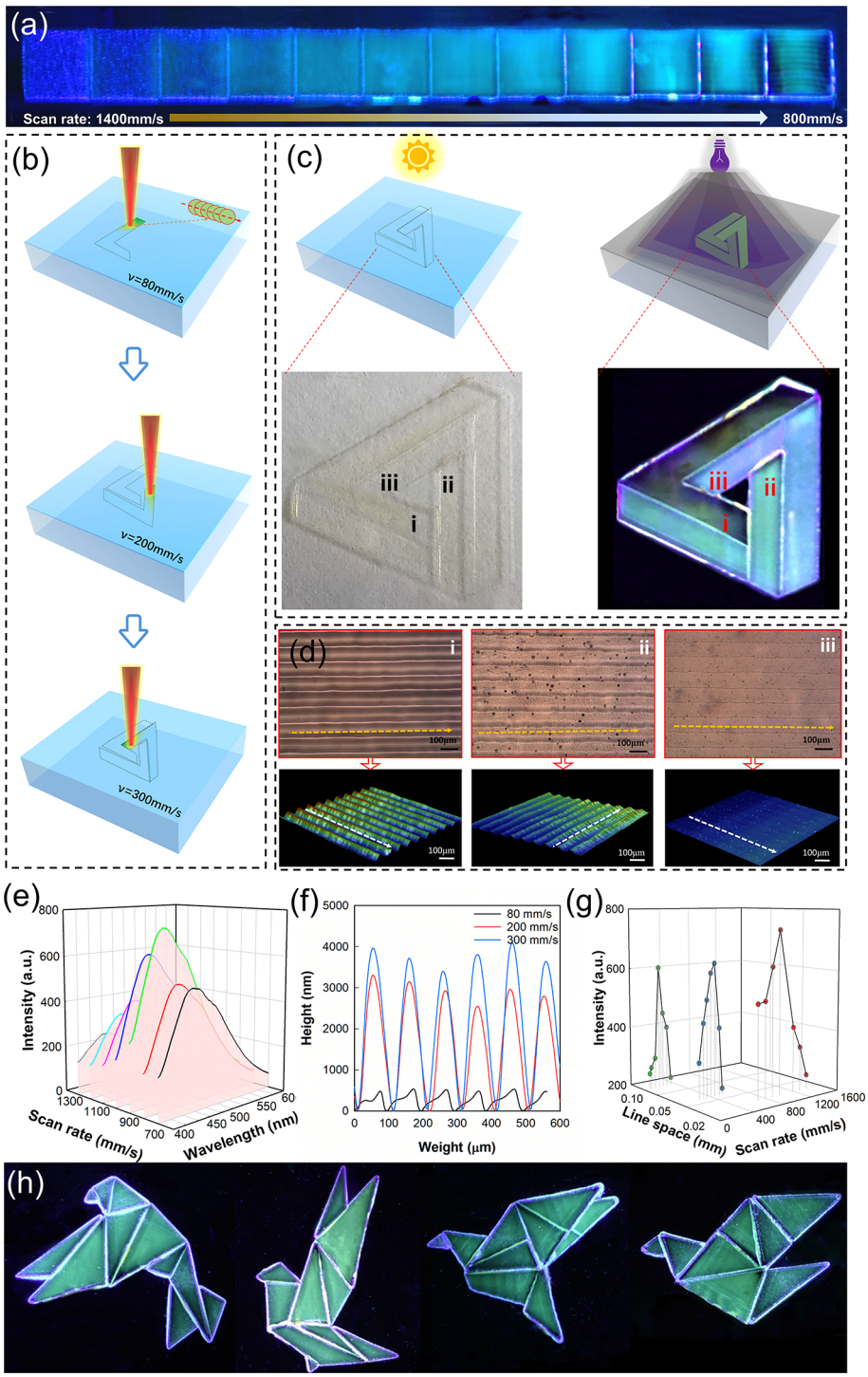

Figure 1. (a) Fluorescent intensity gradient from at a scan rate ranging from 1400 to 800 mm/s at laser power 4 W, 25 kHz, and line space 0.02 mm. (b) Schematic of *in situ* laser direct writing fluorescent pattern on CAB film. (c) Three-dimensional fluorescence triangle pattern formed by different fluorescent intensity sections under daylight and UV light. (d) Microscope image (up) and 3D profile (down) of the "finger-print" microstructure on different positions with various fluorescent intensities: i, scan rate 80 mm/s; ii, scan rate 200 mm/s; and iii, scan rate 300 mm/s (at laser power 4 W, frequency 25 kHz, and line space 0.1 mm); the orange and white arrows shown the laser trace direction. (e) Relationship between scan rate and fluorescent intensity (at laser power 4 W, frequency 25 kHz, and line space 0.02 mm). (f) Height difference with a laser scan rates of 80, 200, and 300 mm/s. (g) Relationship of patterned fluorescence intensity with different laser scan rates and line space under laser power 4 W and frequency 25 kHz. (h) Fluorescent doves by laser direct writing at laser power 4 W, 25 kHz, and with line space 0.02 mm and scan rate 1200 mm/s.

relatively more shallow lines compared with the lines produced at higher scan rates of 200 and 300 mm/s (Figure 1f). The exposed CAB film mainly was melted at a high scan rate (200 mm/s) instead of vaporized due to less heat absorption (Figure 1g). The line-height did not further increase with increasing scan rate (300 mm/s).

The fluorescent intensity of the pattern did not increase linearly with the increase of the line height (Figure 1b-iii). The

https://doi.org/10.1021/acsnano.1c09999
ACS Nano 2022, 16, 2910−2920

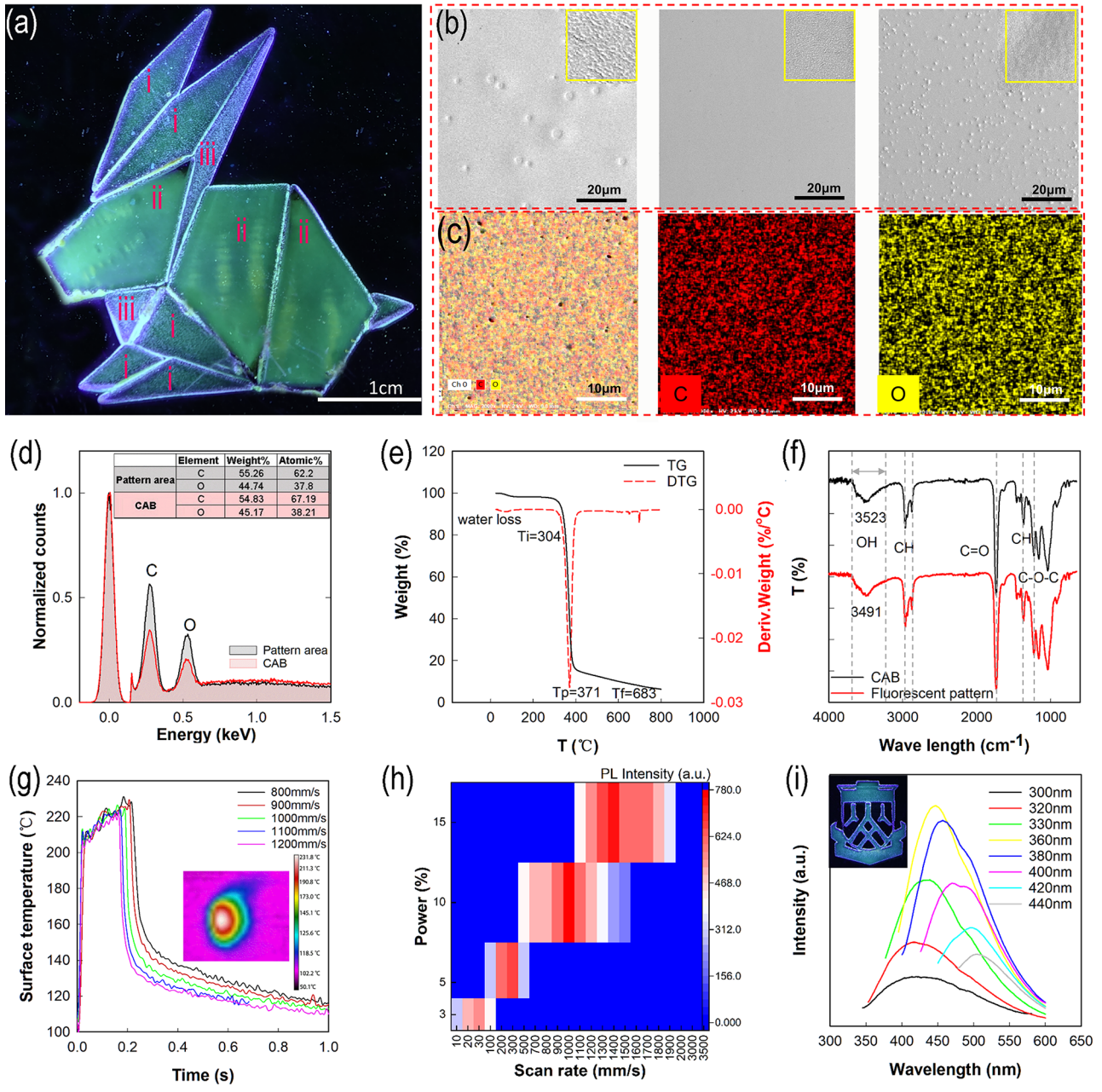

Figure 2. (a) Laser direct written fluorescent rabbit that different parts with different scan rates (i, 800 mm/s; ii, 1000 mm/s; and iii, 1300 mm/s) with laser power 4 W, frequency 25 kHz, and line space 0.02 mm. (b) Scanning electron microscopy (SEM) image of fluorescence patterning area under different scan rates: i, 800 mm/s; ii, 1000 mm/s; and iii, 1300 mm/s; the inset shows the SEM image at 20 kX. (c) Element distribution on the laser patterned CAB surface. (d) Energy dispersive spectroscopy (EDS) of pristine CAB film and laser patterned surface. (e) Thermogravimetric analysis (TGA) of CAB powder. (f) FTIR spectrum of CAB film with and without the laser direct writing process; the dash line indicates the location of each peak. (g) Surface temperature distribution during laser directing writing on the CAB film from a scan rate of 800−1200 mm/s, with laser power 4 W, frequency 25 kHz, and line space 0.02 mm. (h) Solid-state photoluminescence intensity of laser direct written fluorescent patterns (5 mm^2 square) at different laser powers and scan rates with a 0.02 mm line space. (i) Solid-state photoluminescence emission spectrum at the different excitation wavelengths at laser power 4 W, frequency 25 kHz, 0.02 mm line space, and 1200 mm/s. Inset showed the SCNU school badge under 365 nm UV light (the logo was used with permission).

decreased fluorescent intensity could be explained that, as the scan rate further increased, less heat was absorbed by the patterned area and the chemical reaction owing to endothermic absorption in the patterned region decreases, so less fluorescent material is formed. By decreasing the scan line spacing to 0.05 and 0.02 mm, even though the "fingerprint" microstructure disappeared, the adjustable range of the fluorescent intensity became broad (Figure 1g and Figure S2a). The relationship between fluorescence intensity, laser scan rate, and line spacing enables a more vivid image by laser direct writing (Figure 1h and Figure S2b,c). The surface microstructure at the different positions in the fluorescent pattern varies with the laser writing parameters, resulting in different surface reflecting different light intensities, which leads to appearing the distinct color depths. The adjustable surface microstructure and tunable fluorescent intensity of the

https://doi.org/10.1021/acsnano.1c09999
ACS Nano 2022, 16, 2910−2920

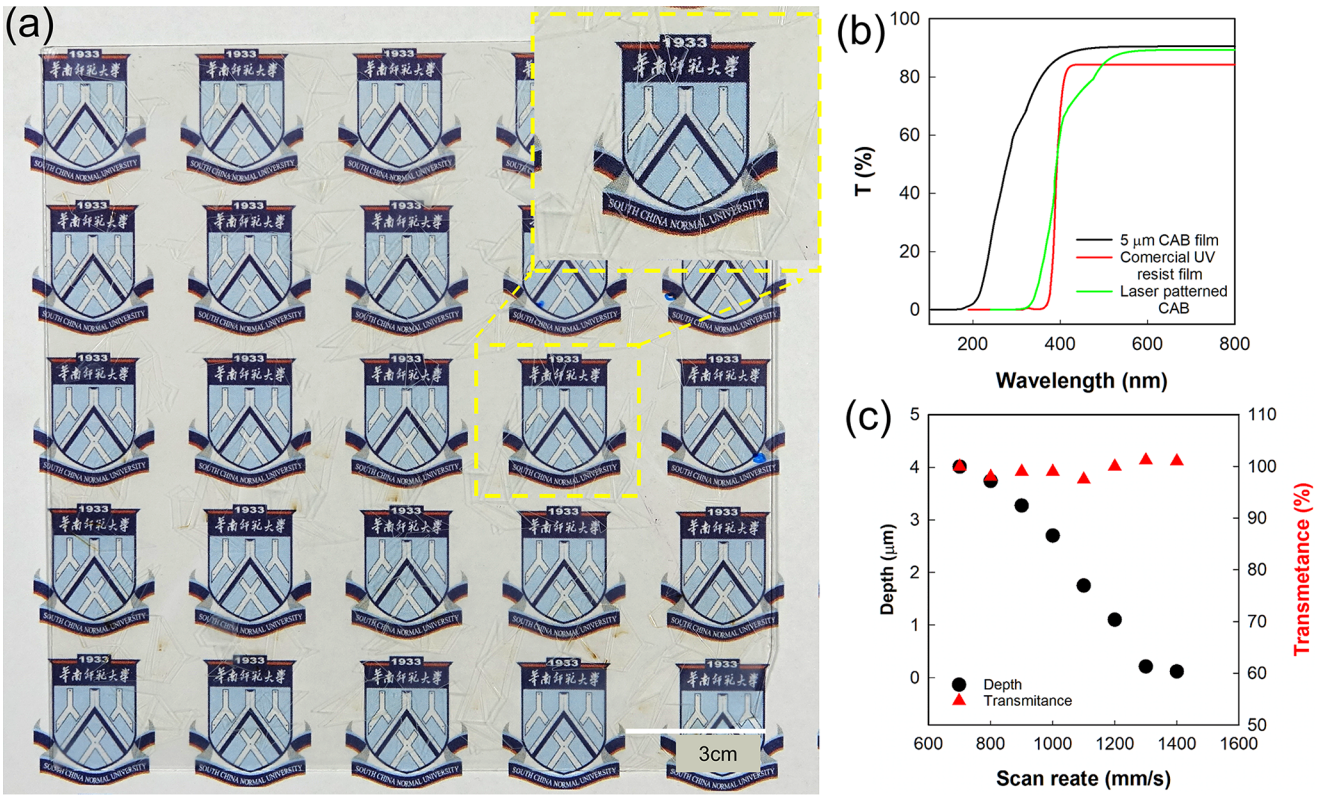

Figure 3. (a) Laser direct writing patterned CAB film on glass plate under daylight; the inset shows the amplified of the patterned area. (b) Comparison of UV-resistant property of laser direct writing CAB pattern (green line), bare CAB film (black line), and commercial UV-resistant film (red line). (c) Relation of ablation depth and transmittance of the laser patterned area with scan rates at laser power 4 W, frequency 25 kHz, and 0.02 mm line space.

fluorescent patterns can effectively enhance the anti-counterfeiting function.

The surface morphology of the laser patterned area was also related to the scan rate under particular conditions. As shown in Figure 2a, a rabbit pattern was drawn with 0.02 mm line spacing (4 W 25 kHz), where different parts draw with variable scan rates. The porous morphology on the film surface was induced by fast gas emission due to a large amount of CAB decomposed at a low scan rate (800 mm/s) (Figure 2b-i). As the scan rate increased (>1000 mm/s), chemical reactions dominated in the melted CAB and a fluorescent pattern was consequently formed. In this circumstance, the surface remained smooth with high transmittance (Figures 2b-ii and 3c). A further increased scan rate resulted in an uneven melted surface due to minor heat transformation (Figure 2b-iii). Element distribution on the patterned CAB surface showed that the main components were carbon and oxygen after laser direct writing (Figure 2c). The Fourier transform infrared (FTIR) spectrum of the fluorescent pattern indicated that the laser ablation of CAB in the air did not influence the main composition, where similar results were shown in the study pyrolysis cellulose in O_2 at low temperature (Figure 2f).[55] The peak around 3500 cm^{-1} was the stretching vibration of the CAB alcohol hydroxyl group, where the peaks at 2970 and 2877 cm^{-1} were the asymmetric and symmetric stretching vibration of methyl and methylene groups. Typically, the peak at 1737 cm^{-1} attributes to the carboxyl groups, and the peak at 1366 cm^{-1} was assigned to CH_3 groups.

The peaks at 1226 cm^{-1} belonged to the C—O—C stretching vibration. The high temperature at the CAB film surface accelerated the hydrogen bond broken between C—OH and COOH and decreased the cohesion of glucan chains. The peak between 1500 and 1600 nm is attributed to the stretching vibration of C—C or C═C in the carbon ring. The increasing peak between 1500 and 1600 nm indicated that more carbon-based substances formed at the fluorescence pattern area, consisting of energy dispersive spectroscopy (EDS) of Figure 2d (Figure S3). As a result, molecules on the surface did ring-opening and repoly condensation reactions that produced fluorescent substances. The peaks at 1737 and 1160 cm^{-1} did not change too much, which indicated that the CAB matrix structure was reserved.

The infrared thermal imaging method monitored the surface temperature (patterned area 2 × 2 mm^2) during the laser direct writing process (Figure 2g). Due to the actual beam quality problem, the reflected spot shape differed from the ideal square (inset image). During the laser direct writing process, the temperature of the patterned surface dramatically increased, and the CAB film turned from solid into the viscoelastic body and then fluid as the temperature exceeded the Tg (133 °C) (Figure 2e and Figure S4). The average surface temperature of the patterned area changed in the range 210−230 °C with varied scan rates. The maximum and average surface temperatures of the laser writing area were linearly correlated with the scan rate (Figure S5). Even though the average temperature was below pyrolysis temperature, the instantaneous temperature of each laser pulse was still very high. So, the thermal degradation of CAB occurred on the surface and fluorescent substances formed in the patterned area. The heat transferred between the thin CAB film, the glass substrate and

https://doi.org/10.1021/acsnano.1c09999
ACS Nano 2022, 16, 2910−2920

released vapor was one of the reasons that most of the CAB material stayed in the molten state when the chemical reaction occurred. After the laser beam left, the melted product solidified with the fluorescent substance fixed in the CAB matrix results in solid fluorescence patterns. The thermal decomposition of CAB at a higher energy would induce carbon nanoparticles and carbon microspheres, resulting in the browning of the material and the declining fluorescent intensity and transmittance.[50]

As shown in Figure 2h, the PL intensity increased with increasing laser power, and the fluorescence intensity first increased and then decreased with the increase of the scan rate under the same laser power. On one side, the maximum emission wavelength was 450 nm excited by 360 nm and did not shift with the scan rate. On the other side, as the excitation wavelength increased, the emission of the solid surface fluorescence shifted from 420 to 520 nm, which showed similar excitation wavelength dependence to one of the CD materials (Figure 2i).[56] The distinctive photoluminescent excitation-dependent property could further improve the safety performance of fluorescent patterns as anti-counterfeiting signs.

Notably, it was found that the film transmittance was not significantly changed after laser direct writing, which should benefit its optical applications (Figure 3a). The CAB film surface was etched away during laser direct writing, and the etched depth increased with decreased scan rate. The laser patterned CAB film did not feature 100% transparency due to the increased surface roughness and surface scattering. But, the 80− 90% visible light transmittance could still be considered rather satisfactory for application as transparent packaging materials (Figure 3c). In addition, the UV absorption property of the fluorescent patterns was also changed. Compared with the same thickness pristine CAB film, the laser patterned area has comparable UV light block performance (100−360 nm) with a commercial UV resistant film (Figure 3b).

The as-prepared fluorescent pattern also showed excellent tolerance to acid/base solutions. The fluorescent intensity of the pattern retained above 90% even after soaking the pattern in the acid/base solutions (pH 5−12) for over 30 days (Figure S6). The fluorescent substances were *in situ* formed in the molten CAB layer; the wrapping and protection effect by the excellent chemical stable CAB prevented it from quenching by the buffer solution. The superior chemical and optical stability of the fluorescent pattern will be more conducive to its applications in anti-counterfeiting and information storage.

Characterization of CDs in the Fluorescent Patterns. To find the origin of the fluorescence, the fluorescent material was extracted from the patterned film and the morphology of the fluorescent substance was analyzed. It appeared that there were CDs distributed in the extracted solution. As shown in Figure 4a,b, the average size of CDs was 2.07 nm, with an average lattice space of 0.26 nm. The particle size distribution of CDs is shown in Figure 4c, and the broad size distribution is also reflected by the photoluminescent (PL) spectrum. The PL spectra exhibited an obvious excitation-dependence with a maximum emission at 450 nm (λ_{ex} = 360 nm, Figure 4d). The green fluorescence came from the quantum size effect and the special surface excited state induced by surface functional groups.[56] The peak around 250 nm in the UV−vis spectrum was attributed to the $\pi-\pi^*$ transition of conjugated C═C, where the peak around 320 nm belonged to the n−π^* transition of the carbon-heteroatom double bond (C═O)

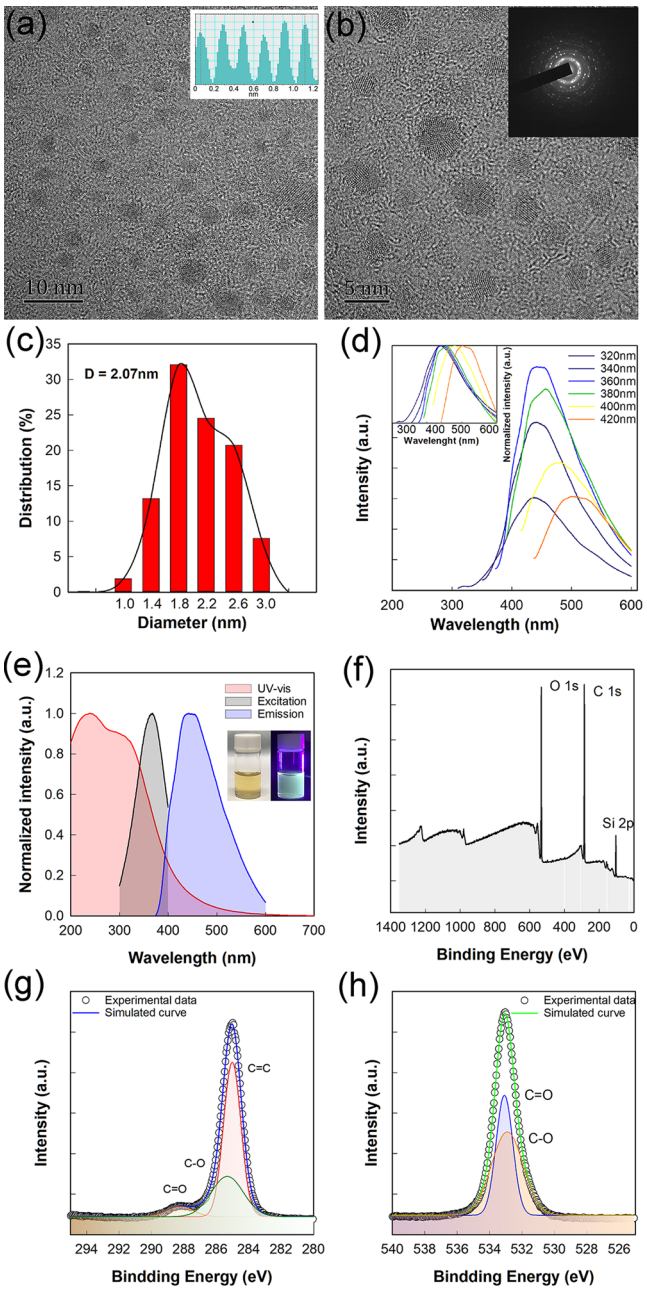

Figure 4. (a and b) TEM image of CDs (inset shows average lattice space of 2.06 nm, electron diffraction spectrum) and (c) the size distribution of CDs. (d) PL emission spectra with different excitation wavelengths (inset: normalized emission intensity curves). (e) UV−vis absorption spectrum (red), PL excitation spectrum (black), and PL emission spectrum (blue); insetof the optical photos of the CDs under daylight and UV light. (f−h) X-ray photoelectron spectroscopy (XPS) of CDs from the fluorescence polymer.

(Figure 4e).[57] The elemental composition of CDs was further analyzed and determined by X-ray photoelectron spectroscopy (XPS) (Figure 4f−h). The main elements were carbon and oxygen. The functional groups at the surface of the CDs were mainly COOH and C═O. The O 1s spectrum was deconvoluted into two peaks centered at 531.2 and 532.4 eV, which should be associated with C—O (hydroxylic groups or ether groups) and C═O (carboxyl groups) (Figure 4f).[58]

https://doi.org/10.1021/acsnano.1c09999
ACS Nano 2022, 16, 2910−2920

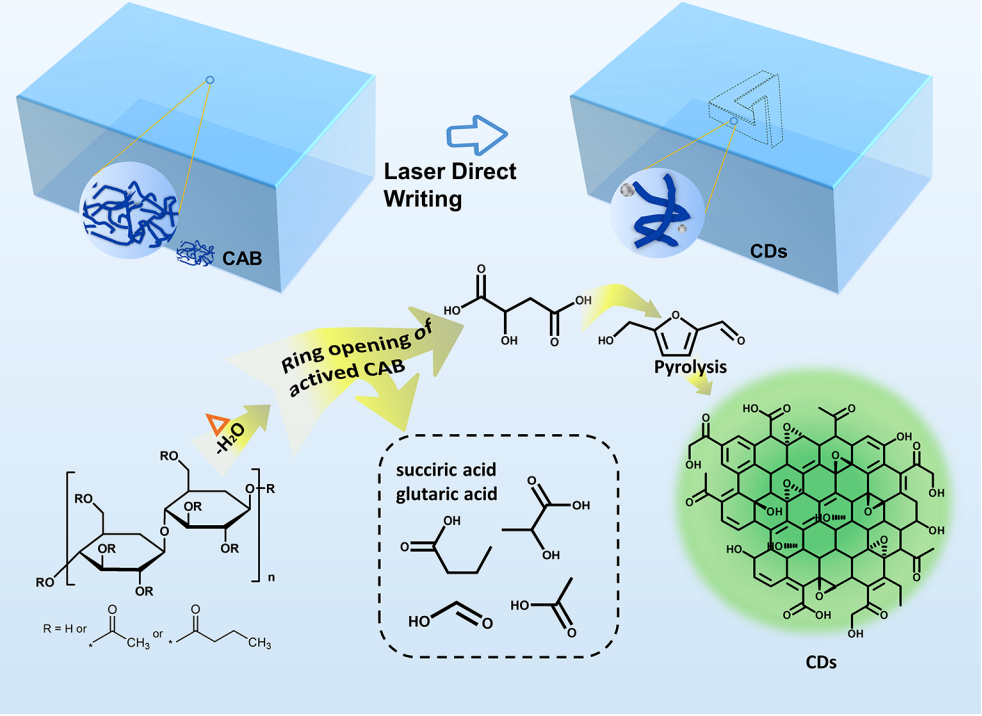

Figure 5. Schematic diagram of the CDs formation from the thermal decomposition of CAB by laser direct writing.

The peaks centered at 285.8 eV (C—O) and 288.3 eV (C═O) deconvoluted from the C 1s spectrum revealed the binding state between C and O atoms in the composite carbon material (Figure 4g).[59] The C═C peak centered at 284.5 eV demonstrating the $\pi-\pi^*$ vibration was observed in the UV−vis spectrum of CDs. Compared with the XPS of CAB, it was evident that the C—OH group was dramatically decreased by laser ablation (Figure S7). It was also illustrated in Figure 5 that the ring-opening reaction of cellulose macromolecule had taken place where the ether groups were reduced. From the solid-state PL emission spectrum, it was clear that the emission of the pattern did not change with scan rate, which indicated that the structure of fluorescent components was not changed with the scan rate. The transmission electron microscopy (TEM) also confirmed that the structure of the fluorescent CDs was not changed with the scan rate (Figure S8).

Formation Mechanism of CDs in the Fluorescent Patterns. Laser ablation of polymer materials has been studied for decades, and various mechanisms have been proposed on the basis of the different material properties and laser sources.[60] In general, the mechanism of laser ablation polymers is mainly regarded as a photophysical process, including photochemical and photothermal reactions. The absorbed light energy is usually converted into heat, which causes the material to melt, vaporize, and decompose. The chemical bonds on the polymer chains are broken by absorbing the photon energy, and the resulting products comprise small molecules, molecular chains, monomers, and polymer fragments. Typically, Qin et al. concluded that the light emission after laser ablation was due to the amounts of luminescent groups (C═C) together with the increased C═C conjugated degree at the polystyrene surface.[42,61] Similarly, Lee et al. claimed that polycyclic aromatic hydrocarbons such as biphenyl, *p*-terphenyl, and substituted naphthalene generated by irradiation on PS were fluorescence sources.[62] Recently, Zheng et al. prepared carbon quantum dots in gold nanoparticle blended PVA film *via* laser ablation.[38] Although it was stated in their work that the C═C bond was detected on the laser-ablated composite surface responsible for the fluorescence, the detailed characterization of CDs was not provided.

Herein, a probable thermal decomposition mechanism from CAB to CDs was proposed on the basis of the finding in this work (Figure 5). Laser writing on the CAB film initially introduced a photothermal effect that resulted in a high localized temperature. After the CAB melted, further increased temperature promoted the photochemical reactions, followed by dehydration and ring-opening reaction afterward. First, the water evaporated and the activated CAB molecules were cross-linked. Further increasing the temperature led to the hydrolyzation of CAB chains to smaller molecules including glucose units. On one side, the as-formed glucose was degraded through ketal or acetal reactions to form organic acids such as butyric acid, acetic acid, formic acid, succiric acid, glutaric acid, and lactic acid.[63,64] The gas components were verified by a gas chromatography−mass spectrometry (GC−MS) chromatogram (Figure S9). The anhydrosugar component of the isomer later forms acetaldehyde, 2-methyl butyrate, vinyl butyrate, 2-propylheptanol, furfural structure, and other small molecule compounds through the opening and cleavage of the C—C bond in the ring.[65,66] On the other side, the ring-opening reaction of CAB or levoglucosan and its equivalents caused the formation of D-hydroxysuccinic acid, which would be the primary precursor of 5-hydroxymethyl-2-furaldehyde (HMF).[67] Further polymerization of HMF produced furan polyester, which would be the precursor of CDs. The carbonation of furan polyesters occurred while the temperature was further raised by laser radiation. The carbon atoms were then reorganized and "recrystallized". As a result, fluorescent CDs eventually formed.[51] Because of the fast laser radiation, not all the CAB went through a decomposition reaction, and after the laser left the patterned area, the melted CAB was cooled with the CDs distributed in the matrix. The functional

https://doi.org/10.1021/acsnano.1c09999
ACS Nano 2022, 16, 2910−2920

groups (COOH or C═O) on the CDs surface would form hydrogen bonds with the hydroxyl groups on the unreacted CAB chain, which was critical for effectively inhibiting the CDs aggregation-induced fluorescence quenching and retaining its solid-state fluorescence characteristics. At this point, the fact that the peaks at ∼3500 cm^{-1} in FTIR spectra shift with increased temperature could be ascribed to the generation of the hydrogen bond between CDs and the CAB chain (Figure 2f).[68]

CONCLUSIONS

In conclusion, we have developed a simple and effective approach for *in situ* writing fluorescence patterns on CAB film using a CO_2 pulse laser under ambient conditions. Under a fixed laser power and frequency (4 W, 25 kHz), the fluorescence intensity and the microstructure of the pattern could be regulated by changing the laser scan rate and line space. In addition to variable fluorescence performance, laser direct-writing films also have excellent UV resistance and stable optical properties. The *in situ* fluorescent patterning mechanism owing to the *in situ* generation of CDs during the laser direct writing of CAB film was proposed and elucidated. Further characterization also verified that the photoluminescence property of the obtained fluorescent pattern has the same excitation dependence as CDs. This technology can produce fluorescent patterns on a large scale with high efficiency and low cost. Obviously, the laser direct writing of fluorescent patterns herein has promising prospects, and it is expected to be applied in the field of bioengineering and information storage in the future.

METHODS AND EXPERIMENTS

CAB Substrate Preparation. Cellulose acetate butyrate (CAB) (butyryl content: 35−39%) was purchased from Aladdin; the material was used as received. Ethyl acetate (99%) and ethanol (99%) were purchased from Sigma-Aldrich and used without further purification. The CAB was first dissolved in ethyl acetate to form a 10 wt % solution. Then, the solution was filtered through a 0.8 μm syringe filter before use. Glass plates were cleaned with ethanol and OR water in ultrasonic for 30 min and then dried at 120 °C for 2 h in an oven. The 10 wt % CAB solution was spin-coated on the glass substrate at 800 rpm, and the dry film thickness was 5 ± 1 μm. Ten micrometers of CAB film was made from a 25 wt % CAB solution for the threshold etching energy density test. The thickness of the transparent film was measured by a DECTEC 3D profiler.

***In Situ* Fluorescent Patterning by Laser Direct Writing and Structural Characterization.** A CO_2 laser labeling machine was used to make fluorescence patterns on the CAB film (Shang Hai Aojian Laser Co., Ltd.). A typical CO_2 pulsed laser with a wavelength of 10.6 μm and a rated power of 40 W was used. For the laser direct writing process, 10% of rated power and 25 kHz frequency were selected. The scan rate and line space were varied to prepare fluorescent patterns with different intensities and surface microstructure. All of the laser writing processes were carried out in the air at room temperature. The patterns were designed by Adobe Photoshop software.

The surface morphology of the pattern areas was examined with scanning electron microscopy (SEM) (ZEISS Gemini 500). The same instrument was also used to acquire EDS to compare the contents of different elements before and after laser direct writing. The solid-state fluorescence spectrum was examined by a Hitachi F-7000 fluorescence spectrometer. The IR spectrum of CAB film and laser patterned film were compared by a Nicolet 6700 Fourier transform infrared spectrometer. The surface temperature distribution was detected by a FLIR A 6700 midwave infrared thermal imager during the laser direct writing process. The glass transition temperature (Tg) was determined by METTLER TOLEDO differential scanning calorimetry with a heating rate of 10 °C/min and a sample size of 5 mg. The thermogravimetric (TGA) curve of CAB was measured by a thermogravimetric analyzer (METTLER).

Characterization of CDs in the Fluorescent Pattern. The fluorescent patterns made by laser direct writing were cut into small pieces and immersed in ethanol to extract CDs. The extraction solution was then concentrated with a rote evaporator and filled into a dialysis bag (RC, molecular weight cut-off: 1000 Da) for 48 h. After dialysis, the solution outside of the dialysis bag was concentrated by a rote evaporator again, and the solution was centrifuged at 10 000 rpm for 10 min. The upper clear liquid was reserved for transmission electron microscope (TEM) testing, respectively. The TEM (JEM-2010, JEOL) was used to observe the morphology of CDs. The photoluminescence (PL) spectra of CDs solutions were performed with a luminescence spectrometer (RF-6000, Shimadzu). A UV−vis spectrophotometer (UV-1750, Shimadzu) recorded the UV absorption and transition in a 10 mm optical path length quartz cuvette. XPS was performed on a Kα X-ray spectrometer (Thermo Fisher Scientific equipped with an Al source, $h\nu$ = 1468.6 eV) to analyze the elemental composition of the CDs.

ASSOCIATED CONTENT

Supporting Information

The Supporting Information is available free of charge at https://pubs.acs.org/doi/10.1021/acsnano.1c09999.

Details of the laser writing process, fluorescent patterns prepared by *in situ* laser writing, characterization of laser-written CAB film and CAB powder, study of surface average temperature during the laser writing process, optical stability of the fluorescent patterns, X-ray photoelectron spectroscopy (XPS) of CAB, transmission electron microscopy (TEM) of CDs produced at different laser scan rates, and analysis of emission gas during the laser direct writing process and figures of pyrolysis gas emission during laser writing process, scan rate and scan time relationship, plot of etch depth vs log (fluence) in laser ablation of CAB, fluorescent patterns, FTIR spectrum, DSC curve, peak and average surface temperature of the laser writing area vs scan rate, solid-state photoluminescence intensity of laser-directed patterned area, X-ray photoelectron spectroscopy patterns, TEM images, and GC−MS spectrum (PDF)

AUTHOR INFORMATION

Corresponding Author

Yao Wang − *Guangdong Provincial Key Laboratory of Optical Information Materials and Technology & Institute of Electronic Paper Displays, South China Academy of Advanced Optoelectronics, South China Normal University, Guangzhou 510006, P. R. China; National Center for International Research on Green Optoelectronics, South China Normal University, Guangzhou 510006, P. R. China;* orcid.org/0000-0002-0713-5018; Email: wangyao@m.scnu.edu.cn

Authors

Yuanyuan Guo − *Guangdong Provincial Key Laboratory of Optical Information Materials and Technology & Institute of Electronic Paper Displays, South China Academy of Advanced Optoelectronics, South China Normal University, Guangzhou 510006, P. R. China; Shenzhen Guohua Optoelectronics Tech. Co. Ltd. & Academy of Shenzhen Guohua Optoelectronics, Shenzhen 518110, P. R. China;* orcid.org/0000-0002-6650-7037

https://doi.org/10.1021/acsnano.1c09999
ACS Nano 2022, 16, 2910−2920

Quan Wang − *Guangdong Provincial Key Laboratory of Optical Information Materials and Technology & Institute of Electronic Paper Displays, South China Academy of Advanced Optoelectronics, South China Normal University, Guangzhou 510006, P. R. China*

Hao Li − *Guangdong Provincial Key Laboratory of Optical Information Materials and Technology & Institute of Electronic Paper Displays, South China Academy of Advanced Optoelectronics, South China Normal University, Guangzhou 510006, P. R. China; National Center for International Research on Green Optoelectronics, South China Normal University, Guangzhou 510006, P. R. China*

Yixun Gao − *Guangdong Provincial Key Laboratory of Optical Information Materials and Technology & Institute of Electronic Paper Displays, South China Academy of Advanced Optoelectronics, South China Normal University, Guangzhou 510006, P. R. China; National Center for International Research on Green Optoelectronics, South China Normal University, Guangzhou 510006, P. R. China;* orcid.org/0000-0001-8617-472X

Xuezhu Xu − *Guangdong Provincial Key Laboratory of Optical Information Materials and Technology & Institute of Electronic Paper Displays, South China Academy of Advanced Optoelectronics, South China Normal University, Guangzhou 510006, P. R. China;* orcid.org/0000-0002-3902-649X

Biao Tang − *Guangdong Provincial Key Laboratory of Optical Information Materials and Technology & Institute of Electronic Paper Displays, South China Academy of Advanced Optoelectronics, South China Normal University, Guangzhou 510006, P. R. China;* orcid.org/0000-0003-3088-038X

Bai Yang − *State Key Lab of Supramolecular Structure and Materials College of Chemistry, Jilin University, Changchun 130012, P. R. China;* orcid.org/0000-0002-3873-075X

Yi-Kuen Lee − *Department of Mechanical & Aerospace Engineering, Hong Kong University of Science and Technology, Kowloon, Hong Kong Special Administrative Region; Department of Electronic & Computer Engineering, Hong Kong University of Science and Technology, Kowloon, Hong Kong Special Administrative Region*

Paddy J. French − *BE Lab, Faculty EWI, Delft University of Technology, Delft 2628CD, The Netherlands*

Guofu Zhou − *Guangdong Provincial Key Laboratory of Optical Information Materials and Technology & Institute of Electronic Paper Displays, South China Academy of Advanced Optoelectronics, South China Normal University, Guangzhou 510006, P. R. China; National Center for International Research on Green Optoelectronics, South China Normal University, Guangzhou 510006, P. R. China; Shenzhen Guohua Optoelectronics Tech. Co. Ltd. & Academy of Shenzhen Guohua Optoelectronics, Shenzhen 518110, P. R. China;* orcid.org/0000-0003-1101-1947

Complete contact information is available at: https://pubs.acs.org/10.1021/acsnano.1c09999

Notes

The authors declare no competing financial interest.

ACKNOWLEDGMENTS

This work was supported by the National Natural Science Foundation of China (Grant No. 51973070 and 51773069), Science and Technology Program of Guangzhou (No. 2019050001), Innovative Team Project of Education Bureau of Guangdong Province, Guangdong Basic and Applied Basic Research Foundation (No. 2021A1515012420), Startup Foundation from SCNU, Guangdong Provincial Key Laboratory of Optical Information Materials and Technology (No. 2017B030301007), and the 111 Project.

REFERENCES

(1) Ma, T.; Li, T.; Zhou, L.; Ma, X.; Yin, J.; Jiang, X. Dynamic Wrinkling Pattern Exhibiting Tunable Fluorescence for Anticounterfeiting Applications. *Nat. Commun.* **2020**, *11*, 1811.

(2) Tan, Y.; Li, R.; Xu, H.; Qin, Y.; Song, T.; Sun, B. Ultrastable and Reversible Fluorescent Perovskite Films Used for Flexible Instantaneous Display. *Adv. Funct. Mater.* **2019**, *29*, 1900730.

(3) Paun, I. A.; Zamfirescu, M.; Mihailescu, M.; Luculescu, C. R.; Mustaciosu, C. C.; Dorobantu, I.; Calenic, B.; Dinescu, M. Laser Micro-Patterning of Biodegradable Polymer Blends for Tissue Engineering. *J. Mater. Sci.* **2015**, *50*, 923−936.

(4) Wang, H.; Ji, X.; Page, Z. A.; Sessler, J. L. Fluorescent Materials-Based Information Storage. *Mater. Chem. Front.* **2020**, *4*, 1024−1039.

(5) Gao, Z.; Han, Y.; Wang, F. Cooperative Supramolecular Polymers with Anthracene-Endoperoxide Photo-Switching for Fluorescent Anti-Counterfeiting. *Nat. Commun.* **2018**, *9*, 3977.

(6) Ding, M.; Dong, B.; Lu, Y.; Yang, X.; Yuan, Y.; Bai, W.; Wu, S.; Ji, Z.; Lu, C.; Zhang, K.; et al. Energy Manipulation in Lanthanide-Doped Core-Shell Nanoparticles for Tunable Dual-Mode Luminescence toward Advanced Anti-Counterfeiting. *Adv. Mater.* **2020**, *32*, 2002121.

(7) O'Banion, C. P.; Yasuda, R. Fluorescent Sensors for Neuronal Signaling. *Curr. Opin. Neurobiol.* **2020**, *63*, 31−41.

(8) Hou, J.; Li, M.; Song, Y. Patterned Colloidal Photonic Crystals. *Angew. Chem., Int. Ed.* **2018**, *57*, 2544−2553.

(9) Song, B.; He, Y. Fluorescent Silicon Nanomaterials: From Synthesis to Functionalization and Application. *Nano Today* **2019**, *26*, 149−163.

(10) Abdollahi, A.; Alidaei-Sharif, H.; Roghani-Mamaqani, H.; Herizchi, A. Photoswitchable Fluorescent Polymer Nanoparticles as High-Security Anticounterfeiting Materials for Authentication and Optical Patterning. *J. Mater. Chem. C* **2020**, *8*, 5476−5493.

(11) Bhunia, S. K.; Nandi, S.; Shikler, R.; Jelinek, R. Tuneable Light-Emitting Carbon-Dot/Polymer Flexible Films Prepared through One-Pot Synthesis. *Nanoscale* **2016**, *8*, 3400−3406.

(12) Senyuk, B.; Behabtu, N.; Martinez, A.; Lee, T.; Tsentalovich, D. E.; Ceriotti, G.; Tour, J. M.; Pasquali, M.; Smalyukh, I. I. Three-Dimensional Patterning of Solid Microstructures through Laser Reduction of Colloidal Graphene Oxide in Liquid-Crystalline Dispersions. *Nat. Commun.* **2015**, *6*, 7157.

(13) Westenhoff, S.; Kotov, N. A. Quantum Dot on a Rope. *J. Am. Chem. Soc.* **2002**, *124*, 2448−2449.

(14) Carayon, C.; Fery-Forgues, S. 2-Phenylbenzoxazole Derivatives: A Family of Robust Emitters of Solid-State Fluorescence. *Photochem. Photobiol. Sci.* **2017**, *16*, 1020−1035.

(15) Bao, B.; Li, M.; Li, Y.; Jiang, J.; Gu, Z.; Zhang, X.; Jiang, L.; Song, Y. Patterning Fluorescent Quantum Dot Nanocomposites by Reactive Inkjet Printing. *Small* **2015**, *11*, 1649−1654.

(16) Wang, F.; Chong, Y.; Wang, F.; He, C. Photopolymer Resins for Luminescent Three-Dimensional Printing. *J. Appl. Polym. Sci.* **2017**, *134*, 44988.

(17) Hou, J.; Zhang, H.; Su, B.; Li, M.; Yang, Q.; Jiang, L.; Song, Y. Four-Dimensional Screening Anti-Counterfeiting Pattern by Inkjet Printed Photonic Crystals. *Chemistry-An Asian Journal* **2016**, *11*, 2680−2685.

(18) Lai, X.; Ren, Q.; Vogelbacher, F.; Sha, W. E. I.; Hou, X.; Yao, X.; Song, Y.; Li, M. Bioinspired Quasi-3d Multiplexed Anti-Counterfeit Imaging Via Self-Assembled and Nanoimprinted Photonic Architectures. *Adv. Mater.* **2022**, *34*, 2107243.

(19) Nam, H.; Song, K.; Ha, D.; Kim, T. Inkjet Printing Based Mono-Layered Photonic Crystal Patterning for Anti-Counterfeiting Structural Colors. *Sci. Rep.* **2016**, *6*, 30885.
(20) Telitel, S.; Morris, J.; Guillaneuf, Y.; Clément, J.-L.; Morlet-Savary, F.; Spangenberg, A.; Malval, J.-P.; Lalevée, J.; Gigmes, D.; Soppera, O. Laser Direct Writing of Arbitrary Complex Polymer Microstructures by Nitroxide-Mediated Photopolymerization. *ACS Appl. Mater. Interfaces* **2020**, *12*, 30779−30786.
(21) Gaižauskas, E. Filamentation versus Optical Breakdown in Bulk Transparent Media. In *3D Laser Microfabrication: Principles and Applications*; Misawa, H., Juodkazis, S., Eds.; Wiley-VCH, 2006; pp 109−138.
(22) Hu, X.; Yang, F.; Guo, M.; Pei, J.; Zhao, H.; Wang, Y. Fabrication of Polyimide Microfluidic Devices by Laser Ablation Based Additive Manufacturing. *Microsystem Technologies* **2020**, *26*, 1573−1583.
(23) Pyo, S.; Son, H.; Choi, K.-Y.; Yi, M. H.; Hong, S. K. Low-Temperature Processable Inherently Photosensitive Polyimide as a Gate Insulator for Organic Thin-Film Transistors. *Appl. Phys. Lett.* **2005**, *86*, 133508.
(24) Srinivasan, R.; Braren, B. Ultraviolet Laser Ablation of Organic Polymers. *Chem. Rev.* **1989**, *89*, 1303−1316.
(25) Dyer, P.; Pervolaraki, M.; Lippert, T. Experimental Studies and Thermal Modelling of 1064- and 532-nm Nd:YVO_4 Micro-Laser Ablation of Polyimide. *Appl. Phys. A: Mater. Sci. Process.* **2005**, *80*, 529−536.
(26) Wang, W.; Lu, L.; Xie, Y.; Mei, X.; Tang, Y.; Wu, W.; Liang, R. Tailoring the Surface Morphology and Nanoparticle Distribution of Laser-Induced Graphene/Co3o4 for High-Performance Flexible Microsupercapacitors. *Appl. Surf. Sci.* **2020**, *504*, 144487.
(27) Yao, Y.; Duan, X.; Niu, M.; Luo, J.; Wang, R.; Liu, T. One-Step Process for Direct Laser Writing Carbonization of Nh 4 H 2 Po 4 Treated Cellulose Paper and Its Use for Facile Fabrication of Multifunctional Force Sensors with Corrugated Structures. *Cellulose* **2019**, *26*, 7423−7435.
(28) Wang, H.; Wang, H.; Wang, Y.; Su, X.; Wang, C.; Zhang, M.; Jian, M.; Xia, K.; Liang, X.; Lu, H.; et al. Laser Writing of Janus Graphene/Kevlar Textile for Intelligent Protective Clothing. *ACS Nano* **2020**, *14*, 3219−3226.
(29) Santos, M. V.; Santos, S. N.; Martins, R. J.; Almeida, J. M.; Paula, K. T.; Almeida, G. F.; Ribeiro, S. J.; Mendonça, C. R. Femtosecond Direct Laser Writing of Silk Fibroin Optical Waveguides. *J. Mater. Sci.: Mater. Electron.* **2019**, *30*, 16843−16848.
(30) Shin, J.; Ko, J.; Jeong, S.; Won, P.; Lee, Y.; Kim, J.; Hong, S.; Jeon, N. L.; Ko, S. H. Monolithic Digital Patterning of Polydimethylsiloxane with Successive Laser Pyrolysis. *Nat. Mater.* **2021**, *20*, 100−107.
(31) Beckham, J. L.; Li, J. T.; Stanford, M. G.; Chen, W.; McHugh, E. A.; Advincula, P. A.; Wyss, K. M.; Chyan, Y.; Boldman, W. L.; Rack, P. D.; Tour, J. M. High-Resolution Laser-Induced Graphene from Photoresist. *ACS Nano* **2021**, *15*, 8976−8983.
(32) Hall, L. S.; Hwang, D.; Chen, B.; Van Belle, B.; Johnson, Z. T.; Hondred, J. A.; Gomes, C. L.; Bartlett, M. D.; Claussen, J. C. All-Graphene-Based Open Fluidics for Pumpless, Small-Scale Fluid Transport Via Laser-Controlled Wettability Patterning. *Nanoscale Horizons* **2021**, *6*, 24−32.
(33) Ismail, A.; El-Newehy, M. H.; El-Naggar, M. E.; Moydeen, A. M.; Menazea, A. Enhancment the Electrical Conductivity of the Synthesized Polyvinylidene Fluoride/Polyvinyl Chloride Composite Doped with Palladium Nanoparticles Via Laser Ablation. *J. Mater. Res. Technol.* **2020**, *9*, 11178−11188.
(34) Barrios, C.; Carrasco, S.; Canalejas-Tejero, V.; López-Romero, D.; Navarro-Villoslada, F.; Moreno-Bondi, M.; Fierro, J.; Capel-Sánchez, M. Fabrication of Luminescent Nanostructures by Electron-Beam Direct Writing of Pmma Resist. *Mater. Lett.* **2012**, *88*, 93−96.
(35) Li, X.; Wang, H.; Shimizu, Y.; Pyatenko, A.; Kawaguchi, K.; Koshizaki, N. Preparation of Carbon Quantum Dots with Tunable Photoluminescence by Rapid Laser Passivation in Ordinary Organic Solvents. *Chem. Commun.* **2011**, *47*, 932−934.
(36) Huang, X.; Guo, Q.; Yang, D.; Xiao, X.; Liu, X.; Xia, Z.; Fan, F.; Qiu, J.; Dong, G. Reversible 3d Laser Printing of Perovskite Quantum Dots inside a Transparent Medium. *Nat. Photonics* **2020**, *14*, 82−88.
(37) Kunwar, P.; Soman, P. Direct Laser Writing of Fluorescent Silver Nanoclusters: A Review of Methods and Applications. *ACS Appl. Nano Mater.* **2020**, *3*, 7325−7342.
(38) Zheng, Y.; Liu, H.; Li, J.; Xiang, J.; Panmai, M.; Dai, Q.; Xu, Y.; Tie, S.; Lan, S. Controllable Formation of Luminescent Carbon Quantum Dots Mediated by the Fano Resonances Formed in Oligomers of Gold Nanoparticles. *Adv. Mater.* **2019**, *31*, 1901371.
(39) Xu, P.; Yanagi, H. Fluorescence Patterning in Dye-Doped Sol-Gel Films by Generation of Gold Nanoparticles. *Chem. Mater.* **1999**, *11*, 2626−2628.
(40) Kunwar, P.; Hassinen, J.; Bautista, G.; Ras, R. H.; Toivonen, J. Sub-Micron Scale Patterning of Fluorescent Silver Nanoclusters Using Low-Power Laser. *Sci. Rep.* **2016**, *6*, 23998.
(41) Kim, E.; Kyhm, J.; Kim, J. H.; Lee, G. Y.; Ko, D.-H.; Han, I. K.; Ko, H. White Light Emission from Polystyrene under Pulsed Ultra Violet Laser Irradiation. *Sci. Rep.* **2013**, *3*, 3253.
(42) Qin, C.-l.; Bai, X.-d.; Zhao, S.-f.; Li, C.-m.; Jiang, H.-j.; Tan, Q. Blue Light Emission from Pulsed Laser Ablated Polyethylene. *Optoelectronics Letters* **2008**, *4* (1), 23−25.
(43) Liu, J.; Geng, Y.; Li, D.; Yao, H.; Huo, Z.; Li, Y.; Zhang, K.; Zhu, S.; Wei, H.; Xu, W.; Jiang, J.; Yang, B. Deep Red Emissive Carbonized Polymer Dots with Unprecedented Narrow Full Width at Half Maximum. *Adv. Mater.* **2020**, *32*, 1906641.
(44) Tao, S.; Lu, S.; Geng, Y.; Zhu, S.; Redfern, S. A.; Song, Y.; Feng, T.; Xu, W.; Yang, B. Design of Metal-Free Polymer Carbon Dots: A New Class of Room-Temperature Phosphorescent Materials. *Angew. Chem., Int. Ed.* **2018**, *57*, 2393−2398.
(45) Ragazzon, G.; Cadranel, A.; Ushakova, E. V.; Wang, Y.; Guldi, D. M.; Rogach, A. L.; Kotov, N. A.; Prato, M. Optical Processes in Carbon Nanocolloids. *Chem.* **2021**, *7*, 606−628.
(46) Ge, M.; Han, Y.; Ni, J.; Li, Y.; Han, S.; Li, S.; Yu, H.; Zhang, C.; Liu, S.; Li, J.; et al. Seeking Brightness from Nature: Sustainable Carbon Dots-Based Aiegens with Tunable Emission Wavelength from Natural Rosin. *Chem. Eng. J.* **2021**, *413*, 127457.
(47) Ji, C.; Zhou, Y.; Leblanc, R. M.; Peng, Z. Recent Developments of Carbon Dots in Biosensing: A Review. *ACS Sensors* **2020**, *5*, 2724−2741.
(48) Wang, Q.; Gao, Y.; Wang, B.; Guo, Y.; Ahmad, U.; Wang, Y.; Wang, Y.; Lu, S.; Li, H.; Zhou, G. S,N-Codoped Oil-Soluble Fluorescent Carbon Dots for High Color-Rendering Wled. *J. Mater. Chem. C* **2020**, *8*, 4343−4349.
(49) Li, L.; Li, Y.; Ye, Y.; Guo, R.; Wang, A.; Zou, G.; Hou, H.; Ji, X. Kilogram-Scale Synthesis and Functionalization of Carbon Dots for Superior Electrochemical Potassium Storage. *ACS Nano* **2021**, *15*, 6872−6885.
(50) Chen, W.; Shen, J.; Lv, G.; Li, D.; Hu, Y.; Zhou, C.; Liu, X.; Dai, Z. Green Synthesis of Graphene Quantum Dots from Cotton Cellulose. *ChemistrySelect* **2019**, *4*, 2898−2902.
(51) Cheng, C.; Xing, M.; Wu, Q. A Universal Facile Synthesis of Nitrogen and Sulfur Co-Doped Carbon Dots from Cellulose-Based Biowaste for Fluorescent Detection of Fe3+ Ions and Intracellular Bioimaging. *Materials Science and Engineering: C* **2019**, *99*, 611−619.
(52) Nawaz, H.; Tian, W.; Zhang, J.; Jia, R.; Yang, T.; Yu, J.; Zhang, J. Visual and Precise Detection of Ph Values under Extreme Acidic and Strong Basic Environments by Cellulose-Based Superior Sensor. *Anal. Chem.* **2019**, *91*, 3085−3092.
(53) Ruan, X.; Wang, R.; Luo, J.; Yao, Y.; Liu, T. Experimental and Modeling Study of CO_2 Laser Writing Induced Polyimide Carbonization Process. *Mater. Des.* **2018**, *160*, 1168−1177.
(54) Biswas, R. K.; Farid, N.; O'Connor, G.; Scully, P. Improved Conductivity of Carbonized Polyimide by CO_2 Laser Graphitization. *J. Mater. Chem. C* **2020**, *8*, 4493−4501.
(55) Gao, T.; Xu, C.; Li, R.; Zhang, R.; Wang, B.; Jiang, X.; Hu, M.; Bando, Y.; Kong, D.; Dai, P.; et al. Biomass-Derived Carbon Paper to Sandwich Magnetite Anode for Long-Life Li-Ion Battery. *ACS Nano* **2019**, *13*, 11901−11911.

https://doi.org/10.1021/acsnano.1c09999
ACS Nano 2022, 16, 2910−2920

(56) Yan, F.; Sun, Z.; Zhang, H.; Sun, X.; Jiang, Y.; Bai, Z. The Fluorescence Mechanism of Carbon Dots, and Methods for Tuning Their Emission Color: A Review. *Microchimica Acta* **2019**, *186*, 583.
(57) Park, S. J.; Yang, H. K.; Moon, B. K. Ultraviolet to Blue Blocking and Wavelength Convertible Films Using Carbon Dots for Interrupting Eye Damage Caused by General Lighting. *Nano Energy* **2019**, *60*, 87−94.
(58) Sun, S.; Zhang, L.; Jiang, K.; Wu, A.; Lin, H. Toward High-Efficient Red Emissive Carbon Dots: Facile Preparation, Unique Properties, and Applications as Multifunctional Theranostic Agents. *Chem. Mater.* **2016**, *28*, 8659−8668.
(59) Hulicova-Jurcakova, D.; Seredych, M.; Lu, G. Q.; Bandosz, T. J. Combined Effect of Nitrogen- and Oxygen-Containing Functional Groups of Microporous Activated Carbon on Its Electrochemical Performance in Supercapacitors. *Adv. Funct. Mater.* **2009**, *19*, 438−447.
(60) Dyer, P. E. Excimer Laser Polymer Ablation: Twenty Years On. *Appl. Phys. A: Mater. Sci. Process.* **2003**, *77*, 167−173.
(61) Qin, C.; Bai, X.; Zhao, S.; Li, C. Blue Light Emission from Pulsed Laser Ablated Polystyrene. *Polym.-Plast. Technol. Eng.* **2009**, *48*, 310−312.
(62) Lee, H. M.; Kim, Y. N.; Kim, B. H.; Kim, S. O.; Cho, S. O. Fabrication of Luminescent Nanoarchitectures by Electron Irradiation of Polystyrene. *Adv. Mater.* **2008**, *20*, 2094−2098.
(63) Yan, L.; Qi, X. Degradation of Cellulose to Organic Acids in Its Homogeneous Alkaline Aqueous Solution. *ACS Sustainable Chem. Eng.* **2014**, *2*, 897−901.
(64) Adolfsson, K. H.; Hassanzadeh, S.; Hakkarainen, M. Valorization of Cellulose and Waste Paper to Graphene Oxide Quantum Dots. *RSC Adv.* **2015**, *5*, 26550−26558.
(65) Chavan, V.; Kalsi, P.; Nadkarni, V.; Pandey, A. Determination of Track Registration Efficiency and Radiation Chemical Yield for Loss of Ester Bonds Due to Gamma Rays in Cellulose Acetate Butyrate (Cab) Nuclear Track Detector. *J. Radioanal. Nucl. Chem.* **2010**, *286*, 181−183.
(66) Winogradoff, N. X-Ray Irradiation of Cellulose Acetate. *Nature* **1950**, *165*, 72.
(67) Román-Leshkov, Y.; Chheda, J. N.; Dumesic, J. A. Phase Modifiers Promote Efficient Production of Hydroxymethylfurfural from Fructose. *Science* **2006**, *312*, 1933−1937.
(68) Alghamdi, M. M.; El-Zahhar, A. A. Cellulose Acetate Butyrate Graphene Oxide Nanocomposite Membrane: Fabrication, Characterization, and Performance. *Chem. Ind. Chem. Eng. Q.* **2021**, *27*, 35−44.

https://doi.org/10.1021/acsnano.1c09999
ACS Nano 2022, 16, 2910−2920